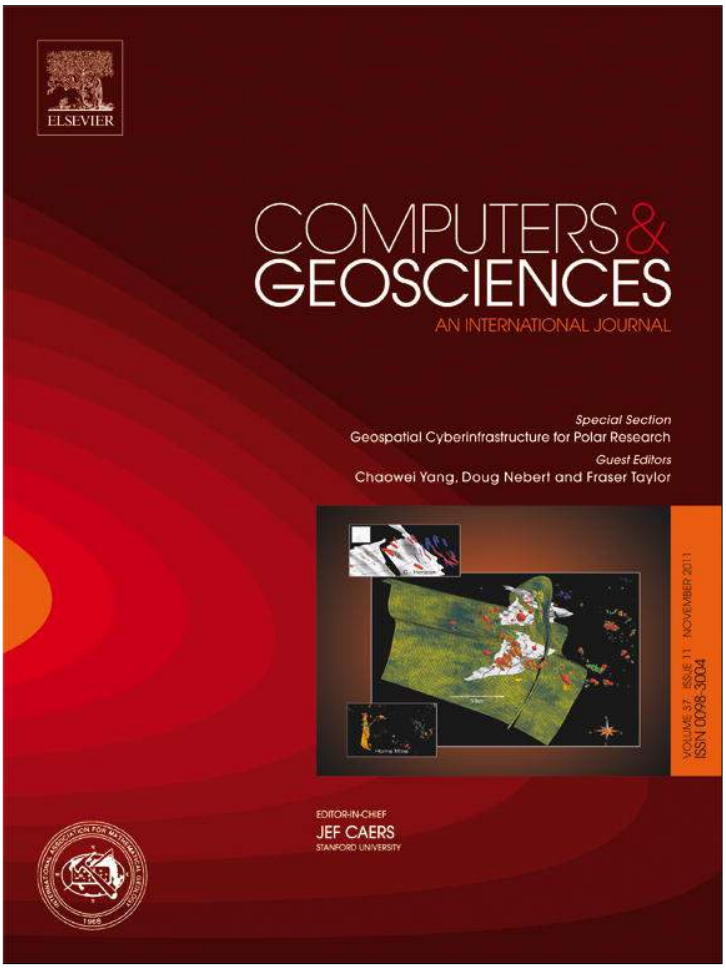

Computers & Geosciences 37 (2011) 1763–1776

Contents lists available at ScienceDirect

Computers & Geosciences

journal homepage: www.elsevier.com/locate/cageo

CSimMDMV: A parallel program for stochastic characterization of multi-dimensional, multi-variant, and multi-scale distribution of heterogeneous reservoir rock properties from well log data ☆

Jun-Wei Huang [a,*], Gilles Bellefleur [b], Bernd Milkereit [a]

[a] University of Toronto, 60 St. George Street, Toronto, ON, Canada, M5S1A7
[b] Geological Survey of Canada, 615 Booth Street, Ottawa, ON, Canada, K1A 0E9

ARTICLE INFO

Article history:
Received 10 August 2010
Received in revised form
17 November 2010
Accepted 19 November 2010
Available online 15 December 2010

Keywords:
Conditional simulation
Random medium
Monte Carlo Simulation
Gas hydrate
Reservoir heterogeneity
Parallel kriging

ABSTRACT

We present CSimMDMV, a software package to simulate two- and three-dimensional, multi-variant heterogeneous reservoir models from well logs at different characteristic scales. Based on multi-variant conditional stochastic simulation, this software is able to parameterize multi-dimensional heterogeneities and to construct heterogeneous reservoir models with multiple rock properties. The models match the well logs at borehole locations, simulate heterogeneities at the level of detail provided by well logging data elsewhere in the model space, and simultaneously honor the correlations present in various rock properties. It provides a versatile environment in which a variety of geophysical experiments can be performed. This includes the estimation of petrophysical properties and the study of geophysical response to the heterogeneities. This paper describes the theoretical basis of the approach and provides the details of the parallel implementation on a Linux cluster. A case study on the assessment of natural gas hydrate amount in Northwest Territories, Canada is provided. We show that the combination of rock physics theory with multiple realizations of three-dimensional and three-variant (3D–3V) gas hydrate reservoir petrophysical models enable us to estimate the average amount of gas hydrate and associated uncertainties using Monte Carlo method.

1. Introduction

Reservoir heterogeneity is the term describing the spatial distribution of dissimilar rock properties in the earth medium. In a conventional oil reservoir, the heterogeneity of elastic properties at the scale of 10–100 m influences the seismic image of resources whereas the heterogeneity of permeability at the scale of <10 m affects the recovery of oil. In addition, reservoirs are rarely defined by a single variable and their characterization usually requires a variety of techniques each sensing different rock properties and each property has different degrees of statistical correlations with others. For example, compressional wave velocity is usually positively and strongly correlated with shear wave velocity, whereas the correlation of density to resistivity or porosity to permeability is often not straightforward. The purpose of CSimMDMV is to model the different scales of spatial variation of multiple rock properties in three dimensions. The simulated heterogeneous petrophysical models honor different degrees of correlations between variables, match the well logs at the borehole locations, and include heterogeneity at the detail of well logs elsewhere in the modeling domain.

A variety of geostatistical methods have been developed to simulate multi-dimensional reservoir heterogeneities (Chilès and Delfiner, 1999). Primarily, these methods fall into two categories: conditional and nonconditional simulation. Nonconditional simulation can only mimic the stochastic properties of the data and do not reproduce the measured data. In comparison, the conditional simulation is able to honor the observations and from this perspective it is a better choice for integrating multi-variant information. Conventional conditional simulation methods of continuous random functions include Sequential Gaussian (e.g., Alabert and Massonnat, 1990), Matrix Decomposition (Davis, 1987), Turning Bands (Matheron, 1973), and Discrete Spectral methods (Shinozuka, 1987). Sequential Gaussian and Matrix Decomposition methods can directly condition the model with measurements, whereas others such as Turning Band and Discrete Spectral methods must employ an additional kriging step to honor the data (Journel, 1974; Delfiner, 1976). In theory, the sequential simulation can match not only the covariance but also the spatial distribution. In practice, however, the conditional probabilities can be easily calculated only for the ideal case of Gaussian random functions (Ripley, 1987). In addition, the sequential procedure cannot easily take advantage of current parallel

Abbreviations: 3D–3V, three-dimensional and three-variant; ACF, auto-correlation function; CSimMDMV, Software abbreviation for conditional simulation of multi-dimensional and multi-variant models; PDF, probability density function; PSDF, power spectrum density function

☆ Code available from server at http://www.junweihuang.info/CompGeophy4Publish.zip.

* Corresponding author. Present address: Geological Survey of Canada, 615 Booth Street, Ottawa, ON, Canada, K1A 0E9. Tel.: +1 613 992 4968; fax: +1 613 943 9285.
E-mail address: Jun-Wei.Huang@NRCan.gc.ca (J.-W. Huang).

0098-3004/$ - see front matter © 2010 Elsevier Ltd. All rights reserved.
doi:10.1016/j.cageo.2010.11.012

architectures, and the computation demand significantly grows with the number of simulation points. Several attempts to parallelize sequential simulation methods can be found in Vargas et al. (2007), Mariethoz (2009), Nunesa and Almeida (2010), and High Performance Geostatistics Library (http://hpgl.sourceforge.net/, accessed on October 20, 2010). The Matrix Decomposition method, on the other hand, first expresses the procedure as operations of a covariance matrix and decomposes the covariance matrix afterwards. However, the complexity of the classical method of Matrix Decomposition increases as N^3 (Davis, 1987). The Turning Band method projects independent 1D simulation along lines (i.e. band) to a simulated point in a plane (2D) or a volume (3D), using a formalism similar to back-projection in tomography. Without sequential constraint, the Turning Band method has been successfully parallelized by Ingam and Cornford (2008) and Emery (2008) on Matlab™ platform. Theoretically, this method can simulate a variety of covariance and variogram in multiple dimensions with arbitrary number of simulated points (Matheron, 1973). However this procedure only ensures the predefined covariance on average over the ensemble of simulations instead of each realization. Therefore, extra care must be taken to design the band directions and to eliminate the artificial anisotropy they may introduce in the models.

Many software packages have implemented the above methods on single CPU, such as GSLIB (Deutsch and Journel, 1998) and Gstat (Pebesma, 2004). The object of this study is to develop an alternative program based on spectral method which extends the capability of the spectral-based simulation method (Le Ravalec et al., 2000) by using current computation power offered by parallel computers. The spectral-based simulation method initially used in Huang et al. (2009) has been implemented in our software CSimMDMV. One advantage of the spectral-based method is the computation efficiency inherited from Fast Fourier Transform (FFT). It can simulate in a timely manner an arbitrary number of points in multiple dimensions for a large range of covariance and allows constraining the covariance of the simulated models by the measurements. Although an additional kriging step must be used to condition the model with observations, both the nonconditional simulation and kriging procedures can be easily parallelized to handle large reservoir models (e.g., Gebhardt, 2003; Kerry and Hawick, 1998). With a small-scale CPU cluster, we have successfully simulated $\sim 10^9$ points conditioned on $\sim 10^3$ data points in a reasonable time. Another advantage of the method is that the cross correlation between multiple parameters is automatically handled in the wave number domain by a cross-spectral density matrix used during the nonconditional simulation (Shinozuka, 1987; Huang et al., 2009).

In this paper, we provide a brief review of the theory of spectral-based conditional simulation with kriging operation. We then present a strategy to parallelize the nonconditional simulation and kriging procedures on a distributed memory CPU cluster using Message Passing Interface (MPI). The speed up of this software running on multiple processors is evaluated and discussed. As an example, we use this software to simulate multiple realizations of Three-Dimensional and Three-Variant (3D–3V) rock property models of gas hydrate reservoir on an 18 node cluster. More specifically, P-wave, S-wave, and density logs from the Mallik 5L-38 borehole in Northwest Territories, Canada, are used to construct a 3D heterogeneous model of the gas hydrate distribution. The efficient multiple realizations of reservoir models allow us to estimate the average gas hydrate volume and quantify the associated uncertainty using the Monte Carlo method.

2. Theory

2.1. Spectral-based nonconditional simulation

A multi-dimensional stationary stochastic field is characterized by an Auto-Correlation Function (ACF) and a Probability Density Function (PDF). A spectral-based approach simulation of a one dimension ($n=1$) and one variant ($m=1$) zero mean stationary stochastic process $u(x)$ by $u_0(x)$ is calculated using

$$u_0(x) = \sqrt{\frac{1}{2\pi}} \sum_{k=-\infty}^{\infty} (S_{uu}(k)\Delta k)^{1/2} \cos(kx + \Phi_k), \tag{1}$$

where $S_{uu}(k)$ is the target Power Spectrum Density Function (PSDF), k is the wave number, and Φ_k is the random variable uniformly distributed from 0 to 2π. The constant $\sqrt{1/2\pi}$ depends on the definition of Wiener–Khinchin transform pair (Yaglom, 1986) in Eq. (2). The PDF is then used to transform $u_0(x)$ to a different process with desired mean and variance.

For a multi-variant process, a cross-spectra density matrix must be used instead of a single PSDF to mimic the mutual statistical correlations between variables. The detailed mathematic expressions needed to simulate a multi-dimensional and multi-variant stochastic field can be found in Shinozuka (1987) and Huang et al. (2009). The target multi-dimensional PSDF $S_{uu}(\mathbf{k})$ can be calculated from the ACF $C(r(\mathbf{x}))$ by a Fourier transformation

$$S_{uu}(\mathbf{k}) = \iiint_{\mathbf{x}} C(r(\mathbf{x}))e^{-i\mathbf{k}\cdot\mathbf{x}} d\mathbf{x} \Leftrightarrow C(r(\mathbf{x})) = \frac{1}{(2\pi)^n} \iiint_{\mathbf{k}} S_{uu}(\mathbf{k})e^{i\mathbf{k}\cdot\mathbf{x}}\, d\mathbf{k}, \tag{2}$$

where n corresponds to the Euclidian dimensionality, $r(\mathbf{x})$ is the radius from the original point to the location $\boldsymbol{x}$, a vector in the multi-dimensional stochastic field (e.g., $\boldsymbol{x}=[x, y, z]$ in 3D). Eq. (2) is also known as the Wiener–Khinchin transform pair. For a Three-Dimensional (3D) and Three-Variant (3V) problem, a 3×3 cross-spectra density matrix $\mathbf{S}(\mathbf{k})$ can be assembled from the power spectral density functions of three variants, i.e., $S_{uu}(\mathbf{k})$ of ν_p, ν_s, and ρ

$$\mathbf{S}(\mathbf{k}) = \begin{bmatrix} S_{pp}(\mathbf{k}) & S_{ps}(\mathbf{k}) & S_{pr}(\mathbf{k}) \\ S_{sp}(\mathbf{k}) & S_{ss}(\mathbf{k}) & S_{sr}(\mathbf{k}) \\ S_{rp}(\mathbf{k}) & S_{rs}(\mathbf{k}) & S_{rr}(\mathbf{k}) \end{bmatrix}, \tag{3}$$

where S_{pp}, S_{ss}, and S_{rr} are PSDF of auto-correlation functions of ν_p, ν_s, and ρ, respectively, and $\mathbf{k}=[k_x, k_y, k_z]^T$. The other components of the matrix are determined by the cross-correlations. For instance, $S_{ps}(\mathbf{k})$ is the PSDF of the cross-correlation between ν_p, and ν_s. For the 3D case, assuming that all variants are correlated with each other (i.e., none PSDF in (3) vanishes), the 3D–3V models can be simulated from

$$\begin{aligned}
V_p^{sim}(\mathbf{x}) = {} & \frac{1}{(2\pi)^{3/2}} \sum_{i=-N_x}^{N_x} \sum_{j=-N_y}^{N_y} \sum_{k=-N_z}^{N_z} \sqrt{|S_{pp}|\Delta k_x \cdot \Delta k_y \cdot \Delta k_z} \\
& \times \cos(k_{xi}x + k_{yj}y + k_{zk}z + \theta_{11} + \Phi_{1ijk}) \\
V_s^{sim}(\mathbf{x}) = {} & \frac{1}{(2\pi)^{3/2}} \sum_{i=-N_x}^{N_x} \sum_{j=-N_y}^{N_y} \sum_{k=-N_z}^{N_z} \sqrt{\left|\frac{S_{ps}^2}{S_{pp}}\right| \Delta k_x \cdot \Delta k_y \cdot \Delta k_z} \\
& \times \cos(k_{xi}x + k_{yj}y + k_{zk}z + \theta_{21} + \Phi_{1ijk}) \\
& + \frac{1}{(2\pi)^{3/2}} \sum_{i=-N_x}^{N_x} \sum_{j=-N_y}^{N_y} \sum_{k=-N_z}^{N_z} \sqrt{\left|S_{ss} - \frac{S_{ps}^2}{S_{pp}}\right| \Delta k_x \cdot \Delta k_y \cdot \Delta k_z} \\
& \times \cos(k_{xi}x + k_{yj}y + k_{zk}z + \theta_{22} + \Phi_{2ijk}) \\
\rho^{sim}(\mathbf{x}) = {} & \frac{1}{(2\pi)^{3/2}} \sum_{i=-N_x}^{N_x} \sum_{j=-N_y}^{N_y} \sum_{k=-N_z}^{N_z} \sqrt{\left|\frac{S_{pr}^2}{S_{pp}}\right| \Delta k_x \cdot \Delta k_y \cdot \Delta k_z} \\
& \times \cos(k_{xi}x + k_{yj}y + k_{zk}z + \theta_{31} + \Phi_{1ijk}) \\
& + \frac{1}{(2\pi)^{3/2}} \sum_{i=-N_x}^{N_x} \sum_{j=-N_y}^{N_y} \sum_{k=-N_z}^{N_z} \sqrt{\left|\frac{(S_{sr} - (S_{ps}S_{pr}/S_{pp}))^2}{S_{ss} - (S_{ps}^2/S_{pp})}\right| \Delta k_x \cdot \Delta k_y \cdot \Delta k_z} \\
& \times \cos(k_{xi}x + k_{yj}y + k_{zk}z + \theta_{32} + \Phi_{2ijk}) \\
& + \frac{1}{(2\pi)^{3/2}} \sum_{i=-N_x}^{N_x} \sum_{j=-N_y}^{N_y} \sum_{k=-N_z}^{N_z}
\end{aligned}$$

$$\times\sqrt{\left|S_{rr}-\frac{S_{pr}^2}{S_{pp}}-\frac{(S_{sr}-(S_{ps}S_{pr}/S_{pp}))^2}{S_{ss}-(S_{ps}^2/S_{pp})}\right|\Delta k_x\cdot\Delta k_y\cdot\Delta k_z}$$
$$\times\cos(k_{xi}x+k_{yj}y+k_{zk}z+\theta_{33}+\Phi_{3ijk}), \quad (4)$$

where $|\ .\ |$ is the absolute value operator. In case where the value inside the operator is complex, the corresponding θ_{im} is the argument and none zero by default. The k_{xi}, k_{yj}, and k_{zk} are the discrete wave numbers, and $\Delta k_x\,\Delta k_y$, and Δk_z are the wave number intervals in x, y, and z dimensions, respectively. Φ_1, Φ_2, and Φ_3 are three independent random phases uniformly distributed from 0 to 2π. For simplicity, the dependence of PSDF and θ_{im} on wave number is dropped. The details of the derivation can be found in Huang et al. (2009). The methods based on correlation function used in seismology are identical to the variogram based conventional geostatistical methods in the special case when the random field is second-order stationary (Chilès and Delfiner, 1999; Yaglom, 1986). Thus, we use techniques for variogram estimation to estimate correlation functions in this study.

According to the observations of Holliger and Goff (2003), regardless of the chemical composition, geologic age and tectonic history of the earth medium, the power spectra of any logging data uniformly decay as $1/f^{(0.5-1.5)}$, where f is the spatial frequency. Such data have power law distribution and can be characterized by a von Kármán type PSDF (von Kármán, 1948). The PSDFs of well logs presented in the application section revealed this behavior (Fig. 1). Thus, we selected von Kármán type random media to characterize gas hydrate reservoir heterogeneity. The von Kármán type random media requires three parameters: characteristic scale (a), standard deviation (σ), and Hurst number (v). Fig. 2a shows a few examples of a von Kármán type PSDF with various Hurst number, a unit standard deviation (σ) and a 10 m isotropic characteristic scale or correlation length ($a=a_x=a_y=10$ m). The function behaves as an asymptotic power law at wave numbers larger than 0.1 m^{-1}. The characteristic scale determines the average scale of the heterogeneities whereas the Hurst number (v) controls the richness of small-scale heterogeneities. Fig. 2b illustrates that higher characteristic scales increase the lateral extension of heterogeneity whereas small Hurst numbers increase the level of small-scale heterogeneities. The Hurst number and vertical correlation length (a_z) can be estimated from borehole logs whereas the lateral correlation lengths (a_x and a_y) must be estimated from external sources such as surface seismic data.

The analytical expression for the von Kármán PSDF can be derived from the Fourier transform of the von Kármán correlation function (Goff and Jordan, 1988)

$$C(r(\mathbf{x}))=(1-(1-\delta_r)n_0)\frac{r^v K_v(r)}{2^{v-1}\Gamma(v)},\quad r(\mathbf{x})=\sqrt{\left(\frac{x}{a_x}\right)^2+\left(\frac{y}{a_y}\right)^2+\left(\frac{z}{a_z}\right)^2}, \quad (5)$$

where n_0 accounts the nugget effect (the discontinuity at $r=0$), δ_r is a Kronecker delta, ($\delta_r=1$, when $r=0$ and $\delta_r=0$, when $r\neq 0$), $K_v(r)$ is the modified Bessel function of the second kind, $\Gamma(v)$ is the Gamma function, and v is the Hurst number. The nugget effect is affected by microstructures, measurement errors and in general is not zero (Chilès and Delfiner, 1999). Using Eq. (2), the PSDF in 1D, 2D, and 3D become

$$\begin{aligned}
&\mathbf{1D}: S_{uu}(\mathbf{k})=(1-n_0)\cdot\frac{\Gamma(v+1/2)}{\Gamma(v)}\cdot\frac{(4\pi)^{1/2}a}{(1+a^2k^2)^{v+(1/2)}},\\
&\mathbf{2D}: S_{uu}(\mathbf{k})=(1-n_0)\cdot\frac{4\pi v a_x a_y}{(1+k^2)^{v+1}},\quad |\mathbf{k}|=\sqrt{k_x^2a_x^2+k_y^2a_y^2},\\
&\mathbf{3D}: S_{uu}(\mathbf{k})=(1-n_0)\cdot\frac{(4\pi)^{3/2}a_x a_y a_z}{(1+k^2)^{v+3/2}}\cdot\frac{\Gamma(v+(3/2))}{\Gamma(v)},\\
&\qquad |\mathbf{k}|=\sqrt{k_x^2a_x^2+k_y^2a_y^2+k_z^2a_z^2}
\end{aligned} \quad (6)$$

where k_x, k_y, and k_z are the wave number components, and a_x, a_y, and a_z are the characteristic length scales in 3-D. The stochastic field $u(\mathbf{x})$ can now be constructed using the cross-spectral density matrix consisting of the target PSDF.

2.2. Conditioning by kriging

According to Journel (1974) and Delfiner (1976), nonconditional simulation of random media can be easily conditioned to the known measurements via kriging. The comprehensive theory on kriging and cokriging can be found in Chilès and Delfiner (1999). The approach below is based on this theory.

By knowing the values of $Z(x)$ at locations $x=x_1, x_2, \ldots, x_N$, the value at an arbitrary location x can be best and unbiasly estimated as

$$Z^*(x)=\sum_{i=1}^{N}\lambda_i Z(x_i), \quad (7)$$

where λ_i is the weighting factors and uniquely determined by the covariance, and $Z^*(x)$ is the estimated value of $Z(x)$ at location x, N is the number of measurements.

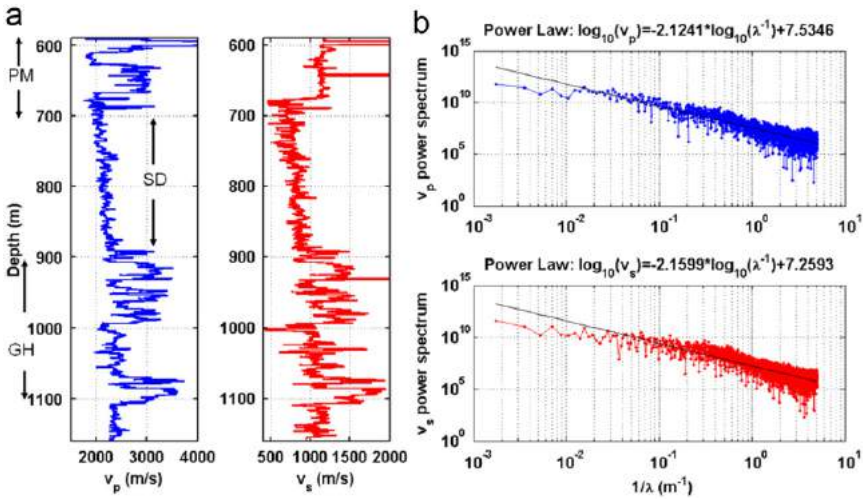

Fig. 1. The power spectra of P- and S-wave sonic logs from Mallik 2L-38 show a power law feature. In the figure, "PM" marks permafrost interval, "SD" water-saturated sediment interval, and "GH" gas-hydrate-bearing sediments.

Now if we rewrite $Z(x)$ as $Z(x)=Z^*(x)+[Z(x)-Z^*(x)]$ and replace the unknown kriging error term $[Z(x)-Z^*(x)]$ on the right hand side by a simulated kriging error $[S(x)-S^*(x)]$, we have

$$Z_s(x)=Z^*(x)+[S(x)-S^*(x)], \tag{8}$$

where $Z_s(x)$ is the conditionally simulated random field, $S(x)$ is the nonconditionally simulated field, and $S^*(x)$ is obtained by kriging using the weights λ_i in Eq. (7). The same weights λ_i are used for $Z^*(x)$ and $S^*(x)$. Thus, the kriging system function only needs to be solved once to perform the two kriging operations. It is straightforward to verify that Eq. (8) can reproduce the actual measurements at $x=x_1$, x_2, …, x_N by letting $x=x_i$. Since $S(x_i)=S^*(x_i)$ and $Z(x_i)=Z^*(x_i)$, thus we obtain $Z_s(x_i)=Z(x_i)$, for all $i=1, 2, \ldots, N$. The conditioned heterogeneous model also has the same covariance as $Z(x)$, which is consistent with the observed data (Chilès and Delfiner, 1999; Delfiner, 1976).

The weighting factors in Eq. (7) can be found by simply minimizing the variance between the estimator Z^* and the target value Z_0

$$E(Z^*-Z_0)^2=E\left(\sum_{i=1}^{N}\lambda_i Z(x_i)-Z_0\right)^2$$

$$=\sum_{i=1}^{N}\sum_{j=1}^{N}\lambda_i\lambda_j E(Z(x_i)Z(x_i))-2\sum_{i=1}^{N}\lambda_i E(Z(x_i)Z_0)+E(Z^2)$$

$$=\sum_{i=1}^{N}\sum_{j=1}^{N}\lambda_i\lambda_j C_{ij}-2\sum_{i=1}^{N}\lambda_i C_{i0}+C_{00}, \tag{9}$$

where we assumed the mean of Z is zero, C_{ij} is the covariance between data $Z(x_i)$ and $Z(x_j)$, C_{i0} is the covariance between data $Z(x_i)$ and the target value Z_0, and C_{00} is the variance of the target value. To minimize Eq. (9), we let the partial derivative of Eq. (9) with respect to the weighting factor λ_i equal to zero. Thus, we have

$$\frac{\partial}{\partial\lambda_i}E(Z^*-Z)^2=2\sum_{j=1}^{N}\lambda_j C_{ij}-2C_{i0}=0. \tag{10}$$

In matrix notation, Eq. (10) is

$$C\boldsymbol{\lambda}=\mathbf{C}_0, \tag{11a}$$

where $\mathbf{C}$ is the matrix of data-to-data covariances and $\mathbf{C}_0$ the vector of covariances between the data and the target value. The vector of

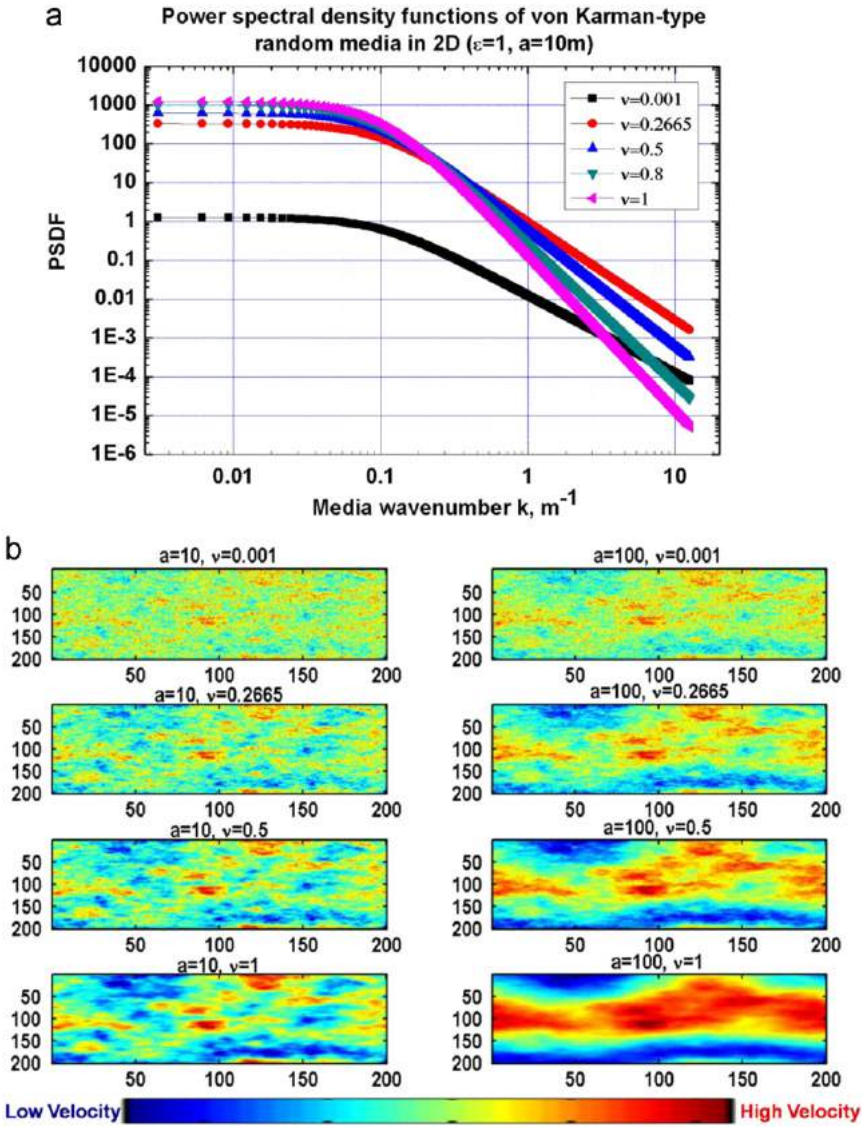

Fig. 2. (a) von Kármán stochastic medium follows a power law at large wave numbers. The standard deviation is $\sigma=1$, and the characteristic scale is $a=a_x=a_y=10$ m. The Hurst number (ν) controls the richness of small-scale heterogeneities shown here as the slope of the power spectral density at large wave numbers and (b) the examples of isotropic 2D random media specified by the von Kármán PDSF in the top panel. The lateral axis is elongated for display purpose.

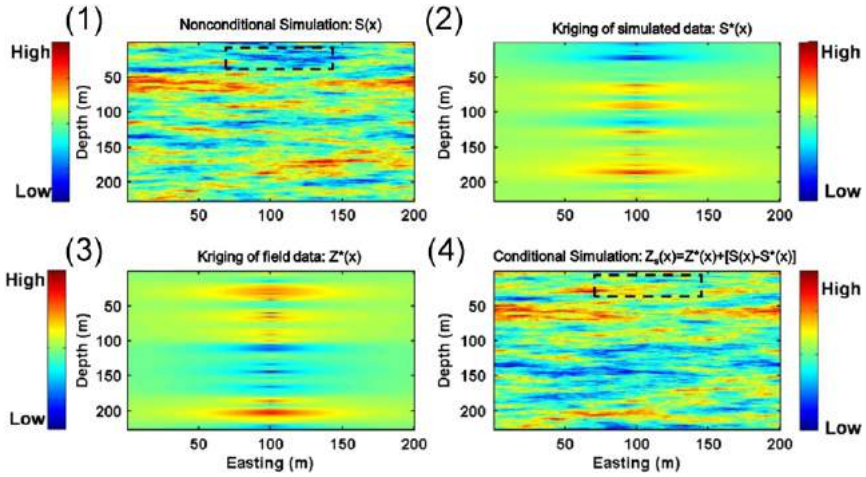

Fig. 3. The intermediate results of conditional simulation demonstrate the performance of kriging of raw data can eliminate the unrealistic values from nonconditional simulations (regions marked by dashed box).

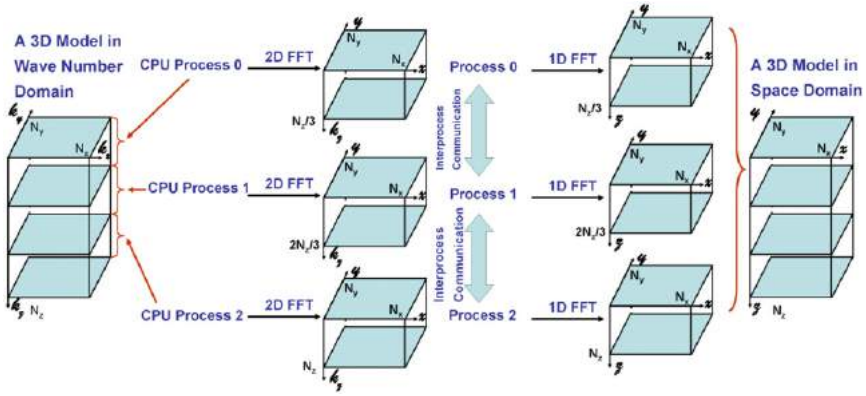

Fig. 4. The schematic illustration of the model construction in parallel. A 3D model with N_x by N_y by N_z grids is first generated in wave number domain and is then divided by the total number of CPU processors (three CPUs in this figure). Each processor applies a 2D FFT along the horizontal directions on a sub-model without interprocessor communication, followed by a 1D inverse FFT to complete the 3D inverse Fourier transform. The final 3D model in space domain is obtained by collecting all sub-models from each processor. See details in the text.

weighting factors $\boldsymbol{\lambda}$ can be solved by

$$\boldsymbol{\lambda} = \mathbf{C}^{-1}\mathbf{C}_0. \tag{11b}$$

Substituting Eq. (11b) into (7), we can express the estimated value in a matrix form

$$Z^* = \boldsymbol{\lambda}^T\mathbf{Z} = \mathbf{C}_0^T\mathbf{C}^{-1}\mathbf{Z}, \tag{12}$$

where $\mathbf{Z}=[Z(x_1),Z(x_2), \ldots, Z(x_n)]^T$, and T denotes matrix transpose.

Fig. 3 illustrates the kriging procedure used to make a non-conditional simulation match measured well log data located in the center of the model. We denote the number of data for kriging using M and N to emphasize that the simulated model can have difference sampling interval from the raw data. Fig. 3 also shows that kriging of raw data can eliminate some unrealistic values from nonconditional simulations.

3. Parallelization

The construction of a multi-dimensional heterogeneous model using spectral-based simulation method that we have presented is straightforward on a single CPU. The computation time, however, increases dramatically with the size of the reservoir model, number of variables, and number of realizations. For instance, multiple realizations (e.g. 100 realizations) of multi-dimension and multi-variant models are required to quantify the uncertainty. In addition, some applications require high resolution models to minimize numerical dispersion and to maintain accuracy of the results. This is the case when models are used to investigate seismic wave propagation in heterogeneous reservoirs (e.g., Huang et al., 2009). Here, we present an implementation of our algorithm on a distributed memory CPU cluster with Message Passing Interface (MPI) for communication between the nodes. The software was written in C/C++ and can be run in both parallel and serial modes. This implementation provides the flexibility to simulate large-scale heterogeneous models in a timely fashion.

3.1. Message passing interface standard

There are two primary parallel programming models which depend on the memory architecture of the hardware, i.e., shared memory and distributed memory (see Grama et al., 2003 and references therein). Shared memory parallel computers allow all processors to access all memory as global address space and significantly reduce the communication time among processors. Models in this category include OpenMP[1] and POSIX® thread (Butenhof, 1997). However, adding more cores onto a single chip can significantly increase the cost of manufacturing and the traffic between shared memory and processors. As a result, the shared memory systems are less scalable than distributed memory

[1] http://openmp.org/wp/

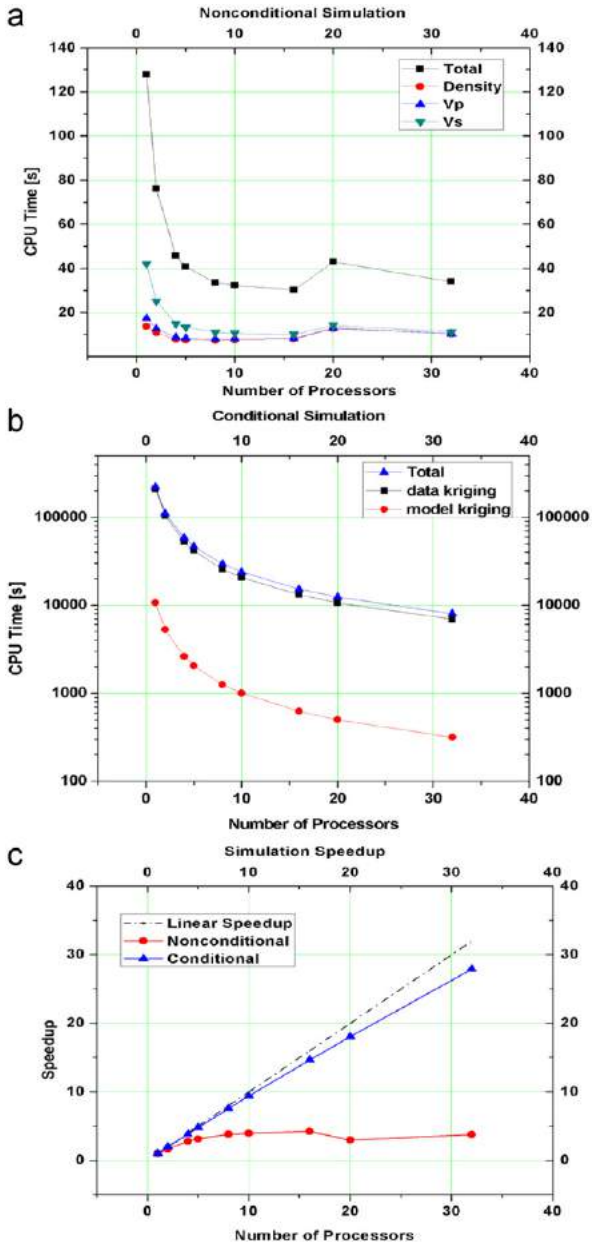

Fig. 5. The CPU time (in second) of both nonconditional and conditional simulation of 3D–3V models. (a) The CPU time of nonconditional simulation of density, υ_p, and υ_s models is dramatically reduced as number of processors increases. The total CPU time (black square) is the summation of the three; (b) the total CPU time (blue triangle) to condition the model with data using simple kriging is the summation of the time for two kriging operations: kriging on the simulated data (red dot) and kriging on the raw data (black square). Note the time scale for kriging operation is in logarithm; and (c) the comparison of the speedup of conditional simulation (blue triangle) with nonconditional simulation (red dot). The dot–dash line is the ideal linear speedup curve. It is obvious that the speed of conditional simulation is close to the ideal case whereas the speedup of the nonconditional simulation reaches the plateau at 16 processors for our specific case. (For interpretation of the reference to color in this figure legend the reader is referred to the web version of this article.)

systems which consist of multiple processors (named nodes), each having its own private memory and sharing data via a communication network. In addition to the high scalability, distributed memory systems can be assembled from off-the-shelf processors and networking devices and thus more cost effective. It is important to mention that our parallel simulation of a high resolution reservoir model on distributed memory system significantly benefits from memory scalability; the memory demand can be easily met by increasing the number of nodes.

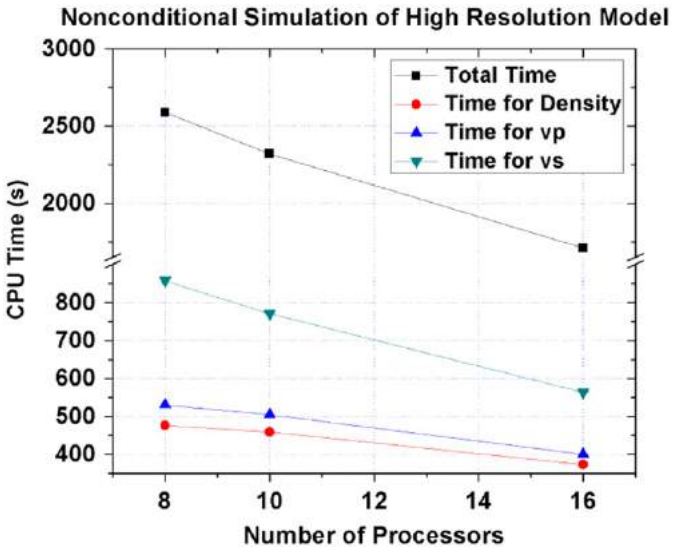

Fig. 6. The computation time of the nonconditional simulation of the high resolution model (3×10^8 points) in parallel mode. Time unit is in second. Due to the limited memory per core on our cluster, the program demands at least 8 cores to deliver the results and the computation time can be reduced by increasing the number of processors.

To facilitate the implementation of data communication on distributed memory systems, MPI, a language-independent library specification for message passing, has been proposed as a standard by a broadly based committee of vendors, implementors, and users (Gropp et al., 1999; Snir and Gropp, 1998). It was designed for high performance computation on both massively parallel machines and on workstation clusters and provides source-code portability of message-passing programs across a variety of architectures. Multiple implementations of MPI are available, for example, MPICH2[2] and LAM/MPI.[3] Recently, LAM/MPI with a few other implementations was merged to form OpenMPI.[4] The details of different implementations can be found on their websites. The spectral-based conditional simulation code was developed on a PC Linux cluster running Local Area Multi-computer (LAM), a MPI implementation for Linux based networks.

3.2. Data decomposition

Two steps are required for the spectral-based conditional simulation (nonconditional simulation and kriging). For the nonconditional simulation, each petrophysical property of the multivariant model is stored as a 3D matrix generated in the wave number domain with Eq. (5). The simulated model is calculated using a multi-dimensional version of Eq. (4), i.e., multi-dimensional inverse Fourier transform to convert data in the wave number domain to the space domain. The model is decomposed and distributed to multiple nodes. Once the cross spectral density matrix of PSDFs of interest is defined, such as a 3 by 3 matrix consisting of PSDF of density (ρ), P-wave velocity (υ_p) and S-wave velocity (υ_s) in Eq. (3), each model can be generated without interactions among processors, which is usually quite expensive and should be minimized. From now on, we only need to focus on decomposition of a single variant model. As shown in Fig. 4, a matrix of N_x by N_y by N_z in the wave number domain is divided by the total number of processors along the k_z direction. Each processor generates a sub-model of N_x by N_y by N_z/n, where n is

[2] http://www.mcs.anl.gov/research/projects/mpich2/index.php
[3] http://www.lam-mpi.org/
[4] http://www.open-mpi.org/

the number of processors. Then each processor can perform a 2D inverse Fourier transform along the k_x and k_y directions on the sub-model without interprocessor communications. Communication between processors is required to complete the inverse Fourier transfer along the last dimension (k_z direction), and the final 3D model in space domain is obtained by collecting all sub-models from each processor. The next step is to condition the resulting model by the measurements via a simple kriging operation using Eq. (6). We adopted the following strategy to parallelize kriging:

I. Distribute **Z** and **C** in Eq. (11) to all processors.
II. Each processor solves equation $\mathbf{C}\boldsymbol{\gamma}=\mathbf{Z}$ for vector $\boldsymbol{\gamma}$.
III. Each processor runs through its sub-model space and calculates $Z^*=\mathbf{C}_0^T\boldsymbol{\gamma}$.
IV. Each processor conditions its sub-model using Eq. (8).
V. Sub-models are collected on the master processor.

Note that each process maintains a copy of $\boldsymbol{\gamma}$ (step II) and performs kriging in a local sub-model (step III) using a locally defined $\mathbf{C}_0$, the vector of covariance between the data and the target value. No interprocessor communication is required until the last step. Sub-models can also be collected on a hard drive and merged into a single file by a single processor.

3.3. Performance results

We tested the program on a Linux (Fedora Core 5, 2.4.26-8smp) cluster of 18 nodes, each having two Intel® Xeon™ dual core CPUs (2.80 GHz) and about 6 gigabyte memory. The nodes are connected through a gigabyte Ethernet switch (1000 Mbps). We evaluate the speedup of the parallel code by constructing a three-dimensional and three-variant (3D–3V) model using different number of processors. In a second assessment, we demonstrate the advantage of parallel platform over serial platform for constructing high resolution reservoir models. On our cluster, we find that 8 processors or more are required to simulate a large model ($\sim 10^8$ grid points).

To evaluate the speedup of the parallelized program, three variant models (ρ, v_p and v_s) of 200 m by 4001 m by 220 m with 2 m grid interval (2.2×10^6 points) are created by running CSimMDMV in both parallel and serial. All models are generated using 1, 2, 4, 5, 8, 10, 16, 20, 32, and 40 processors. The CPU time of nonconditional simulation and kriging procedure is measured as a function of number of processors (Fig. 5). Significant decrease of CPU time can be observed in both operations with higher number of processors. As mentioned before, each variant model can be generated separately and simultaneously, in that case the total CPU time is the longest CPU time required to generate the three models. In this example, models of ρ, v_p, and v_s are constructed in an ordered manner and thus the total CPU time in Fig. 5a is the summation of the CPU time for the nonconditional simulation of the ρ, v_p, and v_s models. To constrain the nonconditional models with well data, two extra kriging steps must be followed: model kriging and data kriging. Fig. 5b shows the total CPU time for the conditional simulation of the ρ, v_p, and v_s models (model kriging) and the kriging of the measurements (data kriging). Kriging of the well log data takes more time simply because logs have significantly higher sampling interval than the models. The speedup of the program is measured as the ratio of the CPU time on a single processor to the time on n processors (Fig. 5c). The conditional simulation scales very well with multiple processors and achieves a close-to-linear speedup up to 40 processors whereas the nonconditional simulation reaches a plateau at 16 processors due to intensive communication during the inverse Fourier transform. Considering that the nonconditional simulation step is a small part of the whole computation, this communication overhead is marginal.

In the second assessment, we constructed a high resolution model of 200 m by 400 m by 226 m at 0.4 m grid interval (approximately 3×10^8 points) for either a simulation of high frequency seismic wave propagation or simply to reproduce the well log sampling interval. A single variant model alone demands 2.1 gigabyte memory using double precision and a total of 16.8 gigabyte for the nonconditional simulation process. On our cluster, due to the limited memory per core, the program requires at least

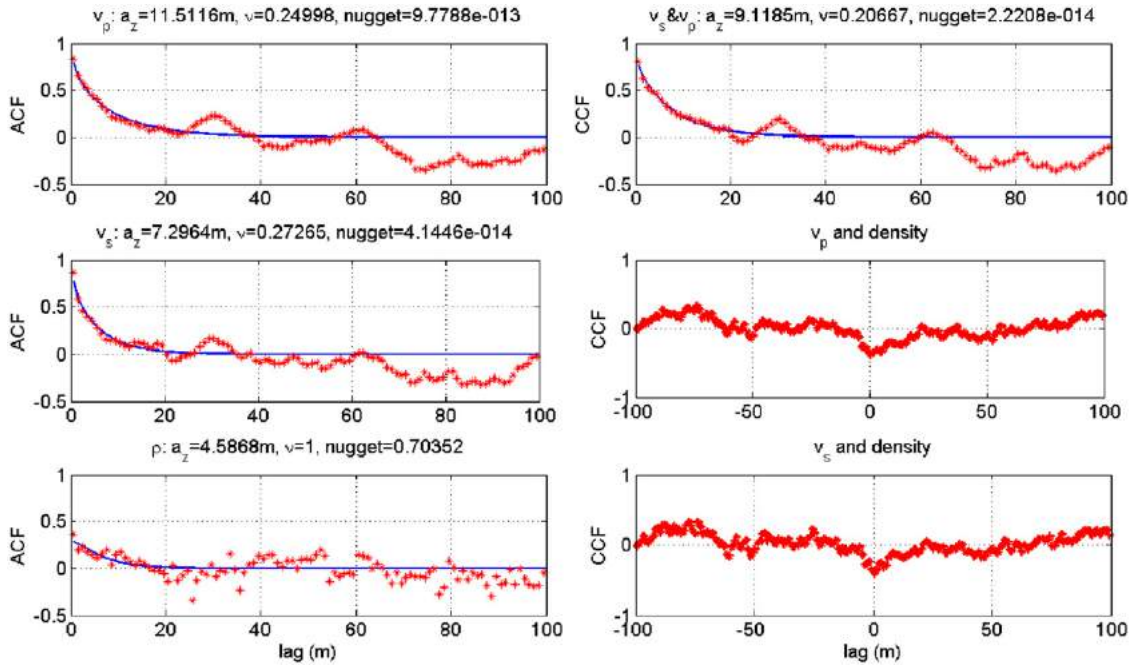

Fig. 7. Least-square regression is used to determine the vertical characteristic scale and the Hurst number, which are listed in the figure. The density logs do not show a strong correlation with velocity logs in the case of gas hydrate formation. Thus, the density is assumed to be uncorrelated with velocities in our model simulation.

8 cores to run in parallel. The calculation time of nonconditional simulation in parallel mode is shown in Fig. 6.

4. Application

In this section, we present an example on how CSimMDMV was used to characterize heterogeneous distribution of gas hydrates at Mallik, Northwest Territories, Canada.

Natural gas hydrates, a type of inclusion compound or clathrate, are composed of gas molecules trapped within a cage of water molecules. Interest in the distribution of natural gas hydrates stems from the hydrate's potential as a future energy source and their possible impact on climate change (Kvenvolden, 1993). The occurrence of gas hydrate in the pore space significantly alters the shear and bulk moduli of the host sediment. Therefore, in this case study, we are interested in three key properties: density, P- and S-wave velocity, as they not only provide information about the hydrate concentration, but also impact seismic wave propagation.

The complete workflow of stochastic characterization of heterogeneous distribution of rock properties of gas hydrate reservoir consists of the combination of the software CSimMDMV with some pre- and post-processing. Briefly it includes the following 7 steps:

Step 1: The background linear trends of v_p, v_s, and density logs are estimated and subtracted.
Step 2: A graphical anamorphosis (Journel, 1974) based on the empirical Cumulative Distribution Function (CDF) is performed to transform the detrended logs with a nonGaussian distribution to a normal distribution to assist the performance of kriging.

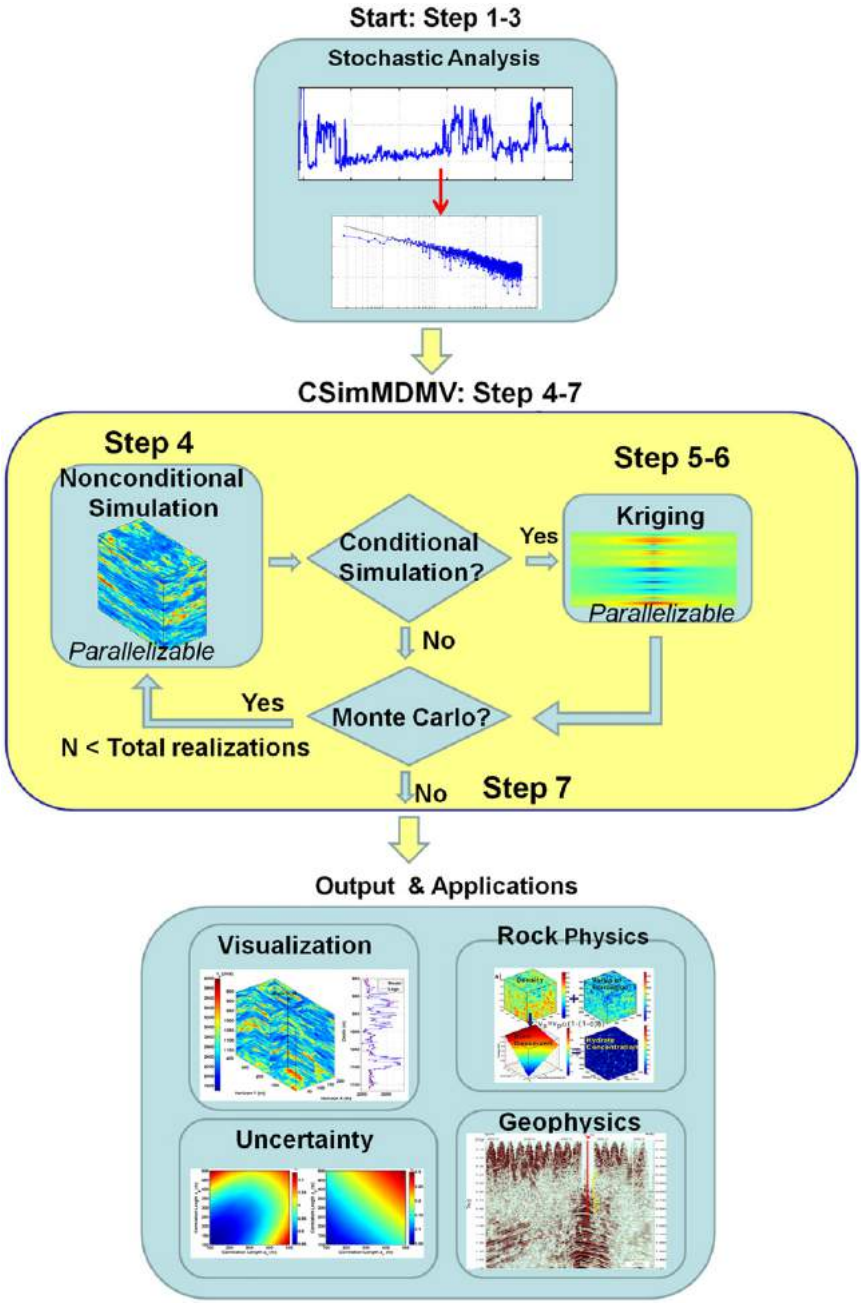

Fig. 8. The workflow of stochastic characterization of multi-dimensional and multi-variant heterogeneous reservoir consists of pre-processing, simulation, and post-processing. The software package CSimMDMV provides the core functions of nonconditional and conditional simulation in either parallel mode or sequential mode.

Step 3: The auto-correlation and the cross-correlation of the well logs are fitted by a von Kármán style correlation function. The fitting results in Fig. 7 show that the cross correlations between velocities and density are rather weak. Due to the fact that the density of gas hydrate is close to the density of fluid, the formation of gas hydrate should not change the density of the sediment as significantly as the shear and bulk moduli. Therefore, we considered velocities as uncorrelated with density in the following steps.
Step 4: The 3D–3V stochastic models are calculated by Eq. (4) with model parameters obtained from step 3. Since the density is uncorrelated with velocities, the spectral density functions of cross correlation are assigned zero.
Step 5: Select the simulated data $S(x_i)$ $(i=1,2,\ \ldots, M)$ at the locations where measurements are available and perform kriging over the whole computation domain using Eq. (5) based on $S(x_i)$, i.e., $S^*(x)=\sum_{i=1}^{M}\lambda_i S(x_i)$;
Step 6: Perform kriging over the whole computation domain using Eq. (5) based on raw data: $Z(x_i)$, i.e., $Z^*(x)=\sum_{i=1}^{N}\lambda_i Z(x_i)$;
Step 7: Obtain the conditional simulation $Z_s(x)$ using Eq. (6). The background trend is then added to the stochastic field after a reverse graphical anamorphosis.

Steps 1–4 are used to build nonconditional models and steps 5–7 further condition the model at the borehole location using the kriging approach. Steps 1–3 are pre-processing performed before launching CSimMDMV, which covers steps 4–7. The pre-processing results such as correlation length and Hurst number must be saved in a text file with specified format to be read by the program. An example of the input file is provided in Appendix A. Post-processing includes, for example, visualization of the model or loading multiple realizations to assess gas hydrate amount. The workflow shown in Fig. 8 summarizes the above seven steps.

An example of such three-dimensional–three-variant (3D–3V) model based on the well logs from gas hydrate bearing sediments at Mallik is shown in Fig. 9, in which the correlations between three variants (ρ, v_p, v_s) are considered simultaneously during the construction of the nonconditional models. Simple visual inspection reveals the strong correlation between v_p and v_s (solid circle) and some subtle uncorrelated features between v_p and v_s (dotted circle) in Fig. 9a and the ideal matching of the simulated model with borehole data at the well location in Fig. 9b. To further evaluate the quality of the simulated models, the histograms of the models and the auto-correlation and cross correlation of the simulated variants are reproduced. They show a very good match with the histograms estimated from the data (Fig. 10a) and honor the predefined von Kármán type correlation functions (Fig. 10b).

4.1. Estimation of gas hydrate volume

The Mallik site has been the subject of several gas hydrate volume assessments (e.g., Collett et al., 1999; Expert Panel on Gas

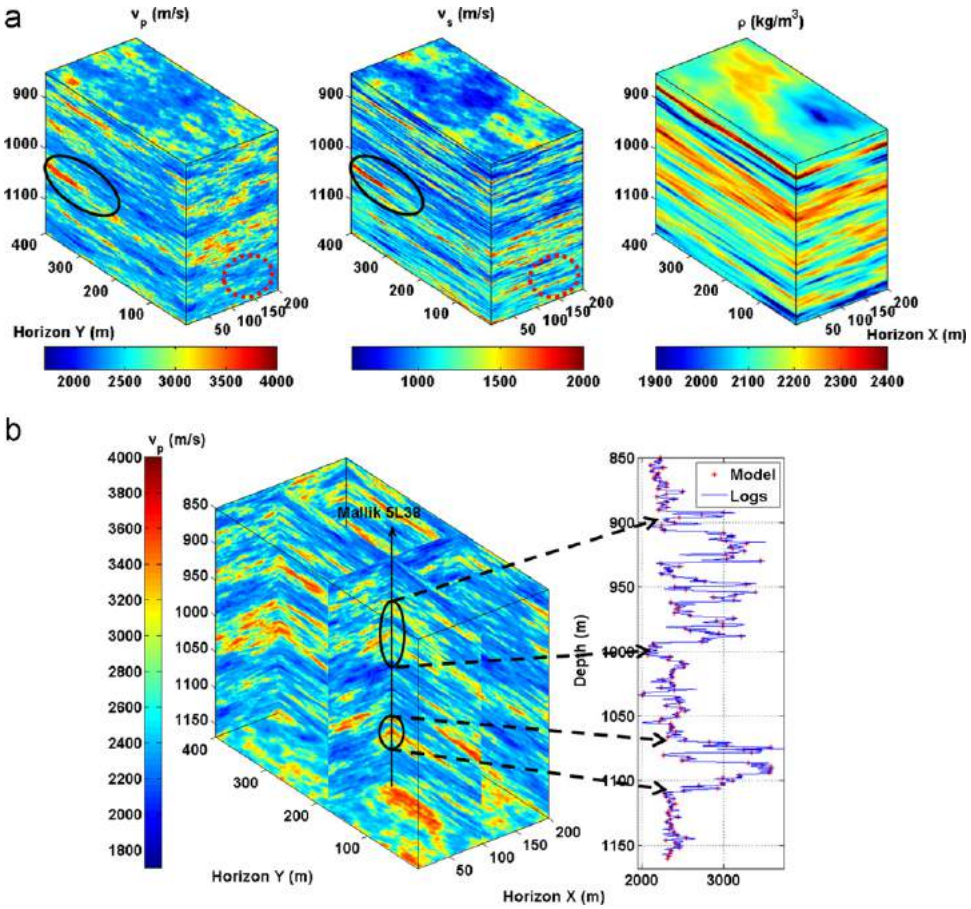

Fig. 9. (a) The simulated 3D–3V heterogeneous reservoir model. The Three Variables (3V) are the density, P- and S-wave velocity. It is observed that the correlated features between v_p and v_s (e.g., solid circle) and uncorrelated subtle features (e.g., dotted circle) are honored simultaneously. The density is not statistically correlated with velocities. This example has the horizontal characteristic scales of $a_x=50$ m and $a_y=100$ m and (b) the conditional simulation of 3D heterogeneous gas hydrate reservoir with borehole Mallik 5L-38 located at the center of the model. The conditionally simulated model ideally matches the log data at the well locations, particularly for the two identified gas hydrate occurrence zones marked by circles.

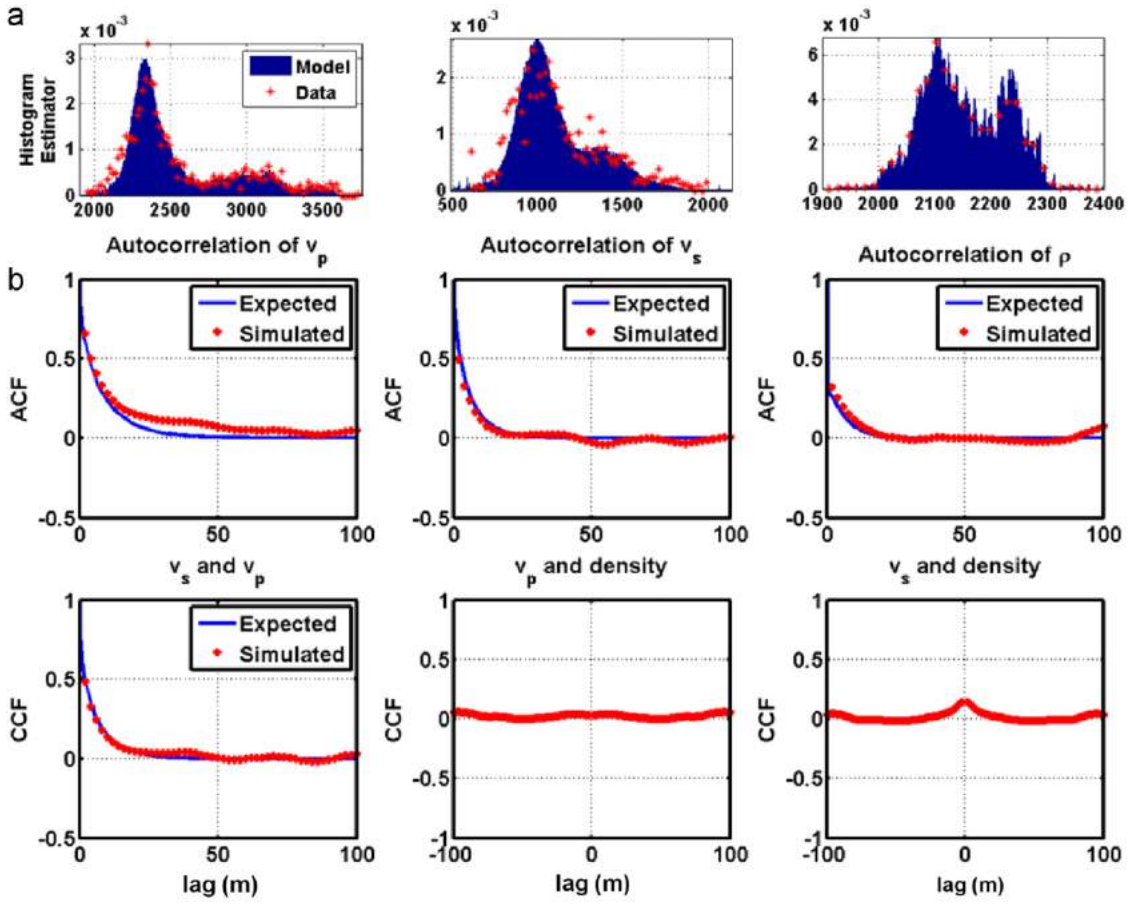

Fig. 10. (a) The histograms of the models are estimated and show the same features as the data histograms and (b) the covariances are estimated and compared with the theoretical von Kármán type covariance function. The correlations between v_p and v_s and uncorrelation between velocities and density are honored and are consistent with the predefined von Kármán type correlation function.

Hydrates, 2008; Bellefleur et al., 2006, 2008). All above assessments are functions of the scale of the seismic wavelength and do not include small scale heterogeneity captured by well logs. Huang et al. (2009) included the log scale heterogeneities by simulating nonconditioned stochastic models of gas hydrate reservoir. With conditional simulation software CSimMDMV, we now reevaluate the amount of gas hydrate using reservoir models consistent with spatial measurement and investigate the impact of external conditioning on the gas hydrate volume estimation.

As illustrated in Fig. 11b, the modified Biot–Gassmann theory (Lee, 2002) established a relationship between the gas hydrate concentration (c), the formation density (ρ), or porosity (φ), and the ratio of the formation velocity (v_s/v_p) for the Mallik region

$$v_s = v_p\alpha(1-(1-c)\varphi), \tag{13a}$$

where α is the velocity ratio of rock matrix

$$\alpha = v_s^M/v_p^M. \tag{13b}$$

We used the superscript M to distinguish from formation velocity: v_p and v_s, which are functions of both c and φ. The porosity is derived from matrix density (ρ_{ma}), fluid density (ρ_{fl}), formation density (ρ), and hydrate concentration

$$\varphi(\rho,c) = \frac{\rho_{ma}-\rho}{(\rho_{ma}-\rho_{fl})(1-c)}. \tag{14}$$

The matrix velocity ratio and matrix density for the modified Biot–Gassmann is calculated using the same elastic moduli as in Lee (2002). The combination of the modified Biot–Gassmann theory with multi-variant models from CSimMDMV provides a way to estimate gas hydrate volume as a function of horizontal correlation length as shown in the work of flow of Fig. 11. First, CSimMDMV generates models of formation velocities and density with vertical correlation length and Hurst number estimated from well logs (Fig. 11a). The elastic models are then used in the modified Biot–Gassmann relationship (Fig. 11b) to estimate gas hydrate concentration (Fig. 11c).

Considering that the gas hydrate concentration is not in a linear relationship with models of ρ, v_p, and v_s (see Eqs. (13) and (14)), the statistical properties of the concentration can be estimated following Monte Carlo simulation of multiple realizations (e.g., 100 realizations) at different correlation lengths (e.g., 100–500 m). The gas hydrate volume is calculated for each realization. The average gas hydrate volume and the corresponding uncertainty are computed as a function of lateral correlation lengths for both conditional and nonconditional models (Fig. 12). Note that we considered the mean value as the average volume and 3 times the standard deviation as the uncertainty with 99.7% confidence limit. As expected, multiple realizations of conditional gas hydrate reservoir models provide less uncertainty on estimated volume compared to nonconditional simulations, whereas the average volume remains similar. As shown in Fig. 12, the average gas hydrate volume and associated uncertainty increase with lateral correlation length. Due to the additional constraint at the borehole, the conditionally simulated models give slightly smaller volume of gas hydrate with less uncertainty than the nonconditional models. For example, the average volume and uncertainty from conditional models with a 500 m correlation

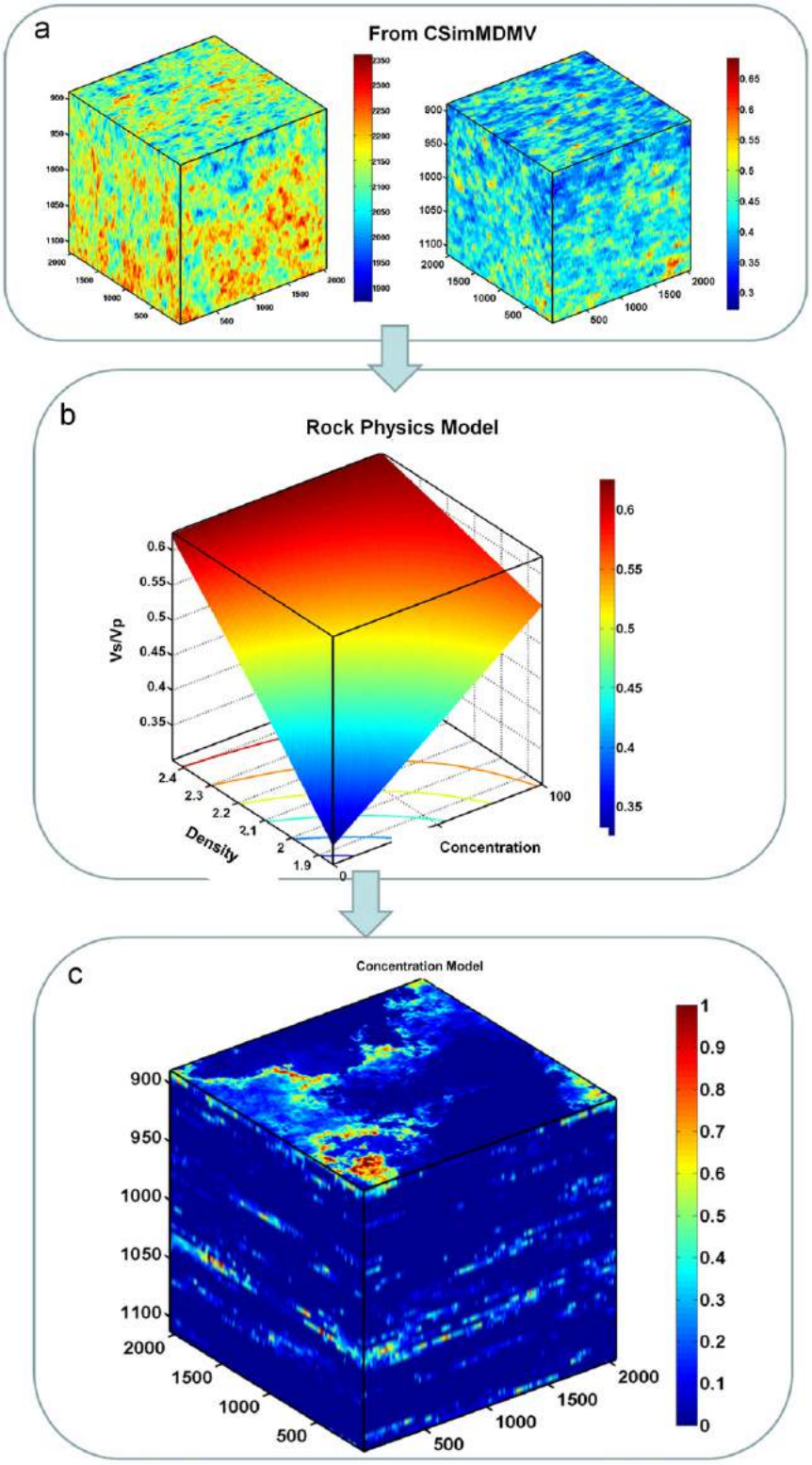

Fig. 11. The workflow of hydrate volume estimation based on the modified Biot–Gassmann theory of Lee (2002) which connects density (kg/m^3) and velocities (m/s) to hydrate concentration; (b) with the three variant models generated by CSimMDMV (a), the hydrate concentration model (c) can be estimated.

length are 1.2% and 0.9%, respectively. Nonconditional simulation with the same correlation length yields an average volume and uncertainty of 1.6% and 1.5%, respectively. Assuming lateral correlation lengths above 100 m but no larger than 500 m, the volume of free gas stored in hydrate from a block of sediments of 500 m $\times$ 500 m $\times$ 226 m is between 9×10^6 and 288×10^6 m^3 from nonconditional models, and between 28×10^6 and 195×10^6 m^3 from conditional models. The lower numbers represent the lowest volume estimated from all realizations with a 100 m correlation length whereas the highest estimates are the largest volume obtained from

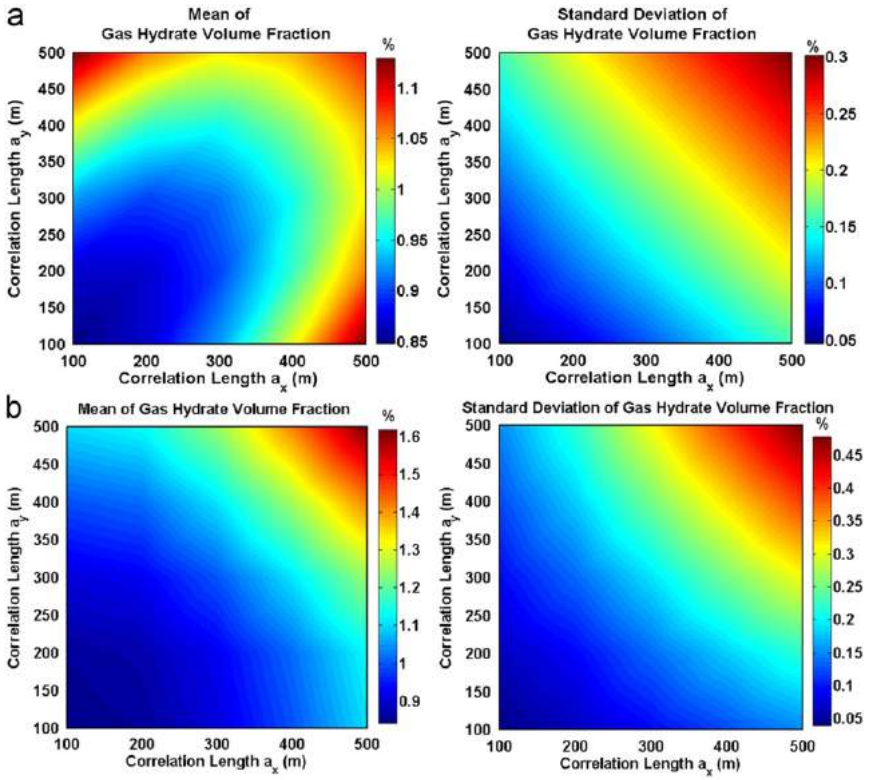

Fig. 12. Mean and standard deviation of gas hydrate volume within a unit rock volume as a function of lateral correlation length using conditional simulation (a) and nonconditional simulation and (b) in (a) the average volume of gas hydrate ranges from 0.85% ± 0.15% to 1.1% ± 0.9%, and in (b) from 0.85% ± 0.15% to 1.6% ± 1.4%, as the lateral correlation length increases from 100 to 500 m. Note that 99.7% confidence limit was used to compute the uncertainty.

realizations with a 500 m correlation length. Our estimated gas hydrate volumes are nearly an order of magnitude lower than earlier estimates made without taking into account effects of heterogeneity. It is important to point out that these results are obtained by conditioning data to a single borehole. Additional boreholes may further reduce uncertainty.

5. Conclusions

This paper describes the theory and performance of CSimMDMV, a software package for the stochastic characterization of multi-dimensional, multi-variant reservoir petrophysical models conditioned by field observations. The software implements both nonconditional and conditional simulation based on spectral method and can run on a distributed memory CPU cluster in both parallel and serial mode. Thus, it extends the capability of conventional spectra-based conditional simulation method to handle large and computationally demanding reservoir models. In the nonconditional simulation, the model is decomposed along the vertical dimension and FFT is applied in parallel to each sub-model. Interprocessor communications are required to complete the transform. The nonconditional simulation reaches the speedup plateau at 16 processors, which is specific to the studied case. The plateau problem is size dependent and it may be reached earlier for a smaller model. In the conditional simulation, an extra kriging operation is performed on the nonconditional model. Due to the parsimonious communication between processors in the kriging step, the parallel program scales very well with multiple processors and achieves a close-to-linear speedup. Faster network connections between nodes may be used to reduce the communication overhead in the nonconditional simulation step. However, observing that most of the computation time was actually spent on kriging, it is more reasonable to employ more processors to further reduce the calculation time. We then demonstrated the applicability of CSimMDMV to simulate a 3D heterogeneous model of the distribution of rock properties of a gas hydrate reservoir at Mallik, Northwest Territories. The combination of rock physics theory with multiple realizations of density, P- and S-wave models of gas hydrate reservoir enables evaluation of gas hydrate resources at the scale of well logs. CSimMDMV can also be applied to simulate heterogeneous models of other physical properties for other applications. More applications of CSimMDMV can be found in Huang et al. (2009, under review).

Acknowledgement

The authors appreciate the helpful suggestions and comments from Kris Vasudevan and Grégoire Mariethoz. We thank Brian Roberts for technical supports on the Linux cluster and for the internal review at Geological Survey of Canada. We acknowledge the international partnership that undertook the Mallik 2002 Gas Hydrate Production Research Well Program: the Geological Survey of Canada (GSC), Japan National Oil Corporation (JNOC), GeoForschungsZentrum Potsdam GFZ), U.S. Geological Survey (USGS), India Ministry of Petroleum and Natural Gas (MOPNG), BP/ChevronTexaco/Burlington joint venture parties, U.S. Department of Energy (USDOE). The GSC contribution number of this article is 20100130.

Appendix A

As described in the application section, three pre-processing steps must be performed to provide the program parameters such as the correlation length, Hurst number, and model dimensions,

etc. This information must be organized in a specific order in a file ready to be used by CSimMDMV. The format of the input parameter file is provided here, followed by an example. The input parameters must be entered into the input file according to the following order:

1. Size of modeling area and sample interval;
2. File name of field data;
3. Number of variants;
4. A flag for nonconditional or conditional simulation;
5. Modeling area original point coordinate;
6. Range of horizontal correlation length;
7. Number of multiple realizations;
8. Vertical correlation length, Hurst number, and nugget effect;
9. Output file head name.
10. A tag to use a rock physic model (only applicable for the gas hydrate model).

Table A1 provides an example of an input parameter file named: CSim3D3V.inp, which was used to simulate the conditional model of gas hydrate reservoir based on logs from one borehole. The details can be found in Huang et al. (2009). Lines that start with "#" are used as annotation and ignored by the program. Users can refer to the documentations included in the software package for more details.

Table A1
An example of input parameter files for CSimMDMV. A 3D–3V case of single realization is assumed.

```
#Input parameter file created by Junwei Huang @ University of Toronto,
  # January 3, 2009
#====================
#Horizon X, Y, top, bottom, and sampling interval (m)
200.0 400.0 850.0 1168.0 2.0
#Number of boreholes and logs file name, X,Y,depth, v1,lv1,v2,lv2, v3,lv3, …
#====================
testlogs.txt
#Number of variants N ≤ 3 for Version V1.1
3
#Switch: nonconditional (0)/conditional (1)
1
#====================
#Origin point x0, y0, and z0
513185   7705619 0
#====================
#ax ay range in meters:
#Start step end
50   50   50
100   50   100
#Maximum Monte Carlo simulations: MaxMC
1
#cdf parameters: az, hurst number, and nugget effect
#C(v1, v1∼Vn), C(v2, V2∼Vn), e.g.,
#C(Vp, Vp),
#C(Vs, Vp),
#C(Vs, Vs),
#C(density, Vp),
#C(density, Vs),
#C(density, density), and
#Must be in the order consistent with v1, v2, and v3,…
#====================
#az (m)                  v           n0
11.5116 0.24998         0
9.1185                  0.20667             0
7.2964                  0.27265             0
0                       0           0
0                       0           0
4.5868                  1.0         0.70352
#===Output file name head string====
test
#===Output Rock Physics Model results tag
0
```

References

Alabert, F., Massonnat, G.J., 1990. Heterogeneity in a complex turbiditic reservoir: Stochastic modeling of facies and petrophysical variability. In: 65th Annual Technical Conference and Exhibition of the Society of Petroleum Engineers New Orleans, Louisiana, SPE paper 20640, pp. 775–790.

Bellefleur, G., Riedel, M., Brent, T., 2006. Seismic characterization and continuity analysis of gas-hydrate horizons near Mallik research wells, Mackenzie Delta, Canada. The Leading Edge 25 (5), 599–604. doi:10.1190/1.2202663.

Bellefleur, G., Riedel, M., Mair, S., Brent, T., 2008. An acoustic impedance inversion approach to detect and characterize gas hydrate accumulations with seismic methods: An example from the Mallik gas hydrate field, Northwest Territories, Canada. In: Proceedings of the Sixth International Conference on Gas Hydrates, Vancouver, B.C., July 6–10, pp. 1–6, 〈http://circle.ubc.ca/handle/2429/1171〉.

Butenhof, D.R., 1997. Programming with POSIX® Threads. Addison-Wesley Professional annotated edition, pp. 400.

Chilès, J.-P., Delfiner, P., 1999. Geostatistics-Modeling Spatial Uncertainty. John Wiley & Sons, Inc, pp. 720.

Collett, T.S., Lee, M.W., Dallimore, S.R., Agena, W.F., 1999. Seismic- and well-log-inferred gas hydrate accumulations on Richards Island. In: Dallimore, S.R., Uchida, T., Collett, T.S. (Eds.), Scientific Results from JAPEX/JNOC/GSC Mallik 2L-38 Gas Hydrate Research Well. Geological Survey of Canada, Bulletin 544, Mackenzie Delta, Northwest Territories, Canada, pp. 357–376.

Davis, M.W., 1987. Production of conditional simulations via the LU triangular decomposition of the covariance matrix. Mathematical Geology 19 (2), 91–98.

Delfiner, P., 1976. Linear estimation of nonstationary spatial phenomena. In: Guarascio, M., Huijbregts, C.J., David, M. (Eds.), Advanced Geostatistics in the Mining Industry, vol. 484. Springer, pp. 49–68.

Deutsch, C.V., Journel, A.G., 1998. GSLIB: Geostatistical Software Library and User's Guide 2nd edition Oxford University Press, pp. 384.

Emery, X., 2008. A turning bands program for conditional co-simulation of crosscorrelated Gaussian random fields. Computers & Geosciences 34 (12), 1850–1862.

Expert Panel on Gas Hydrates, 2008. Energy from gas hydrates: Assessing the opportunities and challenges for Canada, Council of Canadian Academies, ISBN: 978-1-926558-02-8, pp. 222.

Gebhardt A., 2003. PVM kriging with R. In: Proceedings of the Third International Workshop on Distributed Statistical Computing, Vienna.

Goff, J.A., Jordan, T.H., 1988. Stochastic modeling of seafloor morphology: inversion of sea beam data for second-order statistics. Journal of Geophysical Research 93, 13589–13608.

Grama, A., Karypis, G., Kumar, V., Gupta, A., 2003. Introduction to Parallel Computing 2nd edition. Addison Wesley, pp. 656.

Gropp, W., Lusk, E., Skjellum, A., 1999. Using MPI—2nd edition,: Portable Parallel Programming with the Message Passing Interface. The MIT Press, pp. 350.

Holliger, K., Goff, J., 2003. A generic model for the 1/*f*—nature of seismic velocity fluctuations. In: Goff, J.A., Holliger, K. (Eds.), Heterogeneity in the Crust and Upper Mantle: Nature, Scaling, and Seismic Properties 1st edition Springer pp. 358.

Huang, J.-W., Bellefleur, G., Milkereit, B., 2009. Seismic modeling of multidimensional heterogeneity scales of Mallik gas hydrate reservoirs, Northwest Territories of Canada. Journal of Geophysical Research 114 (B07306), 1–22. doi:10.1029/2008JB006172.

Huang, J.-W., Bellefleur, G., Milkereit, B. Stochastic Characterization of Multidimensional, Multi-variant, and Multi-scale Distribution of Heterogeneous Reservoir Rock Properties, Geophyscial Prospecting, under review.

Ingam, B. and D. Cornford, 2008. Parallel geostatistics for sparse and dense datasets. geoENV 2008, Southampton, 8–10 September, 2008.

Journel, A.G., 1974. Geostatistics for conditional simulation of ore bodies. Economic Geology 69 (5), 673–687. doi:10.2113/gsecongeo.69.5.673.

Kerry, K.E., Hawick, K.A., 1998. Kriging interpolation on high-performance computers, Proceedings of the International Conference and Exhibition on High-performance Computing and Networking. Springer, Berlin, Heidelberg pp. 429–438.

Kvenvolden, K.A., 1993. Gas hydrates—geological perspective and global change. Reviews of Geophysics 31 (2), 173–187. doi:10.1029/93RG00268.

Le Ravalec, M., Noetinger, B., Hu, L.Y., 2000. The FFT moving average (FFT-MA) generator: An efficient numerical method for generating and conditioning Gaussian simulations. Mathematical Geology 32 (6), 701–723.

Lee, Myung W., 2002. Biot-Gassmann Theory for Velocities of Gas Hydrate Bearing Sediments. Geophysics 67 (6), 1711.

Mariethoz, G., 2009. A general parallelization strategy for random path based geostatistical simulation methods, Computers & Geosciences, 10.1016/j.cageo.2009.11.001.

Matheron, G., 1973. The Intrinsic Random Functions and their Applications. Advances in Applied Probability 5 (3), 439–468.

Nunesa, R., Almeida, J.A., 2010. Parallelization of sequential Gaussian, indicator and direct simulation algorithms, Computers & Geosciences, 10.1016/j.cageo.2010.03.005.

Pebesma, E.J., 2004. Multivariable geostatistics in S: The gstat package. Computers & Geosciences 30 (7), 683–691.

Ripley, B.D., 1987. Stochastic Simulation. Wiley-Interscience, pp. 264.
Shinozuka, M., 1987. Stochastic fields and their digital simulation. In: Schüeller, G.I., Shinozuka, M. (Eds.), Stochastic Methods in Structural Dynamics. Martinus Nijhoff, Dordrecht, Holland, pp. 93–133, pp. 215.
Snir, M., Gropp, W., 1998. MPI: The Complete Reference, Vol 1: MPI core and Vol 2: MPI-2 Extensions. Massachusetts Institute of Technology Press, Cambridge, Massachusetts, pp. 800.
Vargas, H.s., Caetano, H., Filipe, M., 2007. Parallelization of sequential simulation procedures, Proceedings Petroleum Geostatistics. European Association of Geoscientists Engineers (EAGE), Cascais, Portugal, pp. 5.
von Kármán, T., 1948. Progress in the statistical theory of turbulence. Journal of Marine Research 34 (11), 530–539.
Yaglom, A.M., 1986. Correlation Theory of Stationary and Related Random Functions, vol. I: Basic Results. Springer-Verlag, New York Inc, pp. 516.